ELSEVIER

Journal of Materials Processing Technology 113 (2001) 115–123

Journal of Materials Processing Technology

www.elsevier.com/locate/jmatprotec

The finite element analysis on planetary rolling process

Chih-Kang Shih, Chinghua Hung*, Ray-Quen Hsu

Department of Mechanical Engineering, National Chiao Tung University, 1001 Ta-Hsueh Road, Hsinchu, Taiwan, ROC

Abstract

This paper is focused on using the finite element method to simulate and analyze the planetary rolling process. First, a basic geometric model of the planetary rolling mill that considers roll profiles and offset angle of the rolls was constructed. Then, a three-dimensional elastic–plastic finite element simulation was used to analyze both the deformation characteristics of this process and the distributions of stress and strain in the workpieces. During simulations, an algorithm called Equation of Meshing was proposed by which the initial contact conditions between the rollers and the workpiece were successfully derived. Finally, an optimum design method was integrated into this analysis for seeking the best design variables in order to reduce the cavity conditions in the leading end of milled steel rods.

Keywords: Finite element analysis; Planetary rolling process; Equation of Meshing

1. Introduction

Traditionally, most stainless steel rods are manufactured in the roughing rolling process with large reduction ratio by several 2-high rolling mills. Six to eight conventional mills can be replaced when using one planetary rolling mill (Planetenshrägwalzwerk, PSW as shown in Fig. 1 [1]) in the roughing rolling process. The PSW mainly contains three conical rollers and an external ring. As shown in Fig. 2, the rollers are inclined and are located equally around the axis of the workpiece and their axes intersect that of the workpiece by an offset angle. This offset angle makes the workpiece move forward as the rollers rotate. The rollers are positioned by the ring. The ring encloses the rollers and rotates in the direction opposite to that of the rollers. Besides fixing the rollers, the main purpose of the ring is to counteract the twisting deformation of the workpiece during rolling process and help to keep the rods round after rolling. The usage of PSW decreases the cost of operation and maintenance and reduces the required plant space. Furthermore, the advantages of PSW include flexibility of ingot size, low rolling load, low lateral spread of material [2,3] and a low temperature drop between the leading and trailing end of the rolled bar [4]. These characteristics help to raise the precision, to homogenize the quality and to increase the competitiveness of the products.

There are some reports about the planetary rolling process in the literature. In analytical research, Hwang et al. [5] used the upper bound method and elementary mechanics analysis to analyze the force and torque of the rollers. A dual stream function has been proposed for investigating the plastic deformation behavior of the rod during the planetary rolling process [6]. Most experimental researches conducted the rolling experiments with plasticine, the material properties of which can be adjusted to meet that of stainless steel at elevated temperature. Aoyagi and Ohta [7] observed the flow of the material, the load and torque on the rollers, and the pressure distribution on rollers during rolling process with different cross-section reduction rates. In addition, they studied the influence of the offset angle on the exit velocity of the rods. Nishio et al. [8] discussed the quality characteristics of rolled products with different offset angles and roller profiles. On numerical analysis, Li [9] used the elasto-plastic finite element method to analyze the elementary deformation behavior of the planetary rolling process. However, few researches have been done on completely simulating the planetary rolling process with three-dimensional finite element deformation analysis. The purpose of this study was thus to further analyze the planetary rolling process with finite element simulations and systematically obtain the effects of the rolling parameters. Because the simulation of the planetary rolling process is three-dimensional with the characteristics of non-linearity and large deformation, the numerical calculation demands efficient and powerful software. The vectorized explicit finite element code LS-DYNA3D [10] has thus been selected as the simulation tool.

* Corresponding author. Fax: +886-35-720-634.
E-mail address: chhung@cc.nctu.edu.tw (C. Hung).

0924-0136/01/$ – see front matter
PII: S0924-0136(01)00643-4

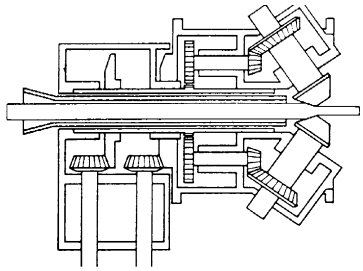

Fig. 1. Cross-section of the PSW (source: [1]).

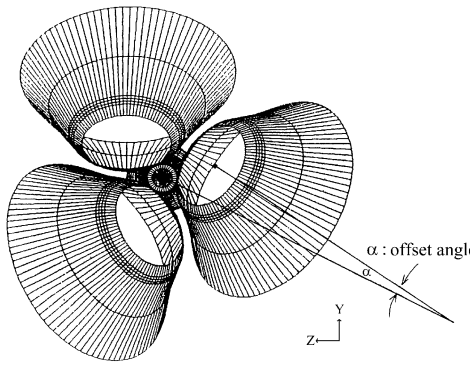

Fig. 2. Roller of PSW (courtesy of Walsin Cartech Specialty Steel).

2. Model of planetary rolling mill

2.1. Simplification of the model

The operation of the PSW includes the revolution of three rollers, the rotation of the rollers and the rotation of the external ring. The major boundary conditions include the contacts between the three rollers and the workpiece and the contacts between rollers and the ring. Thus, a complete and realistic model will make the finite element analysis very complicated. In addition, the control over the rotation of each components and analyses of contacts between each components will cost huge computational time. Therefore, it is reasonable to simplify the simulation model.

The main purpose of the external ring has been explained in the previous section. If the axes of the rollers are fixed and the orbital revolution of the rollers is ignored, the external ring can be omitted from the PSW model. The orbital motion provided by the external ring can be taken care of by the relative motion of the workpiece with free rotational degrees of freedom. Thus, the key points in the analysis of the simplified model contain only the rotation of the rollers and the contact conditions between the rollers and the workpiece.

2.2. Generation of roller profile

For the geometry of the rollers, a third-order polynomial was used to define their profiles. For a point $\boldsymbol{R}_\mathrm{R}$ on a roller,

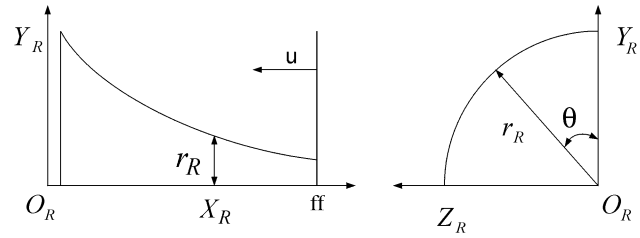

Fig. 3. Roller profile on the coordinate system S_R.

the radius r_R is defined as

$$r_\mathrm{R} = r_\mathrm{R}(x) = ax^3 + bx^2 + cx + d \tag{1}$$

Thus the coordinates of $\boldsymbol{R}_\mathrm{R}$ on the roller's coordinate system S_R can be represented as

$$\boldsymbol{R}_\mathrm{R} = [\,x_\mathrm{R} \quad y_\mathrm{R} \quad z_\mathrm{R} \quad 1\,]^\mathrm{T} \tag{2}$$

where $x_\mathrm{R} = ff - u$, $y_\mathrm{R} = r_\mathrm{R}\cos\theta$, $z_\mathrm{R} = r_\mathrm{R}\sin\theta$, and $ff =$ const.

$$0 \le \theta < 2\pi, \qquad 0 \le u < U, \quad U = \text{const.} \tag{3}$$

Fig. 3 shows the projective profile of the roller on the local roller's coordinate system. Revolution of this curve with respect to the axis X_R makes a complete profile of a roller. The global coordinate system of the simulation model was defined as the coordinate system of the workpiece. The geometric relation between the local coordinate system $S_\mathrm{R}(X_\mathrm{R}, Y_\mathrm{R}, Z_\mathrm{R})$ and the global coordinate system $S_0(X_0, Y_0, Z_0)$ is shown in Fig. 4. Thus, a point $\boldsymbol{R}_\mathrm{R}$ in S_R can be represented as $\boldsymbol{R}_0$ in S_0 by using the coordinate transformation:

$$\boldsymbol{R}_0 = \boldsymbol{M}_{0\mathrm{R}}\boldsymbol{R}_\mathrm{R} \tag{4}$$

The transformation matrix is

$$\boldsymbol{M}_{0\mathrm{R}} = \begin{bmatrix} \cos\beta\cos\alpha & \sin\beta\cos\alpha & -\sin\alpha & 0 \\ -\sin\beta & \cos\beta & 0 & \mathrm{d}r \\ \cos\beta\sin\alpha & \sin\beta\sin\alpha & \cos\alpha & 0 \\ 0 & 1 & 0 & 1 \end{bmatrix} \tag{5}$$

where α represents an the offset angle and β the inclined angle. Through the transformation matrix $\boldsymbol{M}_{0\mathrm{R}}$, the coordinate point $\boldsymbol{R}_0$ becomes:

$$\boldsymbol{R}_0 = [\,x \quad y \quad z \quad 1\,]^\mathrm{T} \tag{6}$$

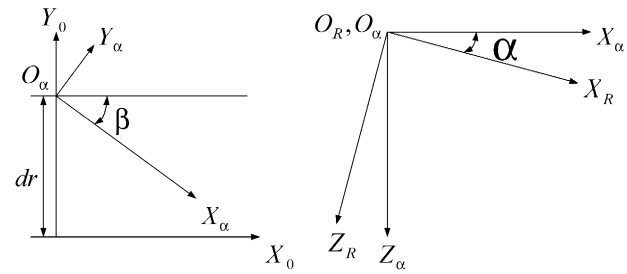

Fig. 4. Relation between the roller coordinate system and the workpiece coordinate system.

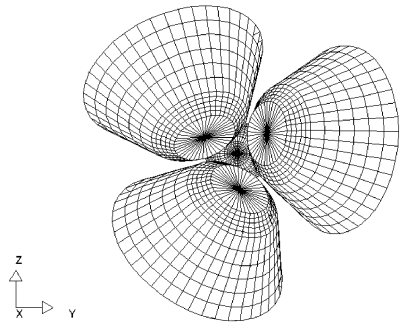

Fig. 5. Mesh system of PSW.

where

$$x = \cos\beta\cos\alpha\, x_R + \cos\alpha\sin\beta\, y_R - \sin\alpha\, z_R$$
$$y = -\sin\beta\, x_R + \cos\beta\, y_R + dr$$
$$z = \cos\beta\sin\alpha\, x_R + \sin\beta\sin\alpha\, y_R + \cos\alpha\, z_R \quad (7)$$

With the above procedures, the authors built all three rollers with 120° separation together with a cylindrical workpiece. Thus a complete model had been established and then the corresponding mesh system could be generated as shown in Fig. 5.

2.3. Material properties

Most experimental work in the references used plasticine as working material. Therefore, in the beginning of analysis, the authors simulated with plasticine for the purpose of comparison. Because no specifications of plasticine were mentioned in the references, plasticine PPW 1/3 1.5 was selected as the working material. Fig. 6 shows the stress–strain relationship of this plasticine [11]. Following this

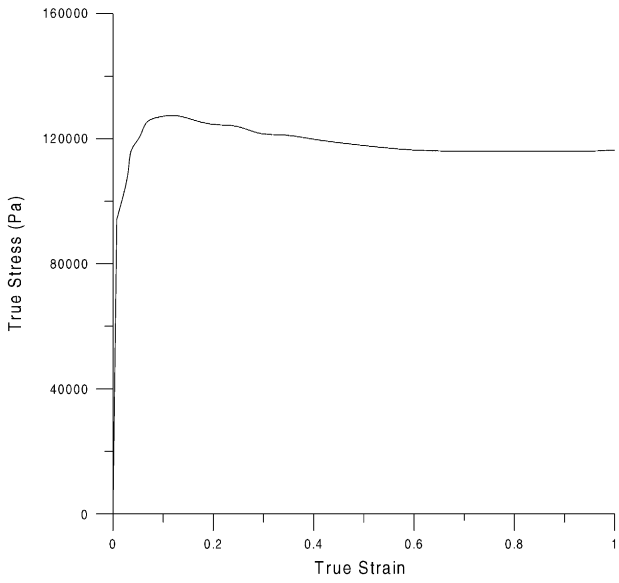

Fig. 6. True-stress–true-strain curve of plasticine PPW 1/3 1.5 (source: [11]).

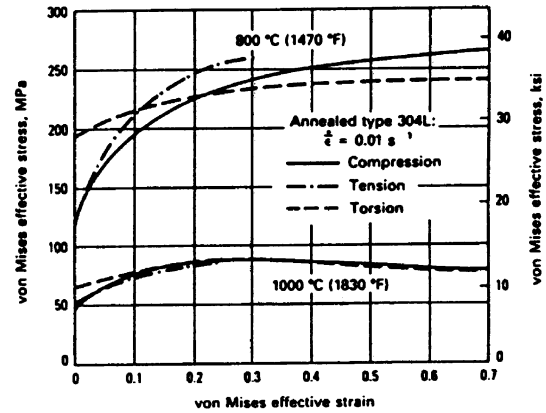

Fig. 7. Effective-stress–effective-strain curve of 304 l stainless steel (source: [12]).

comparison with plasticine, low-alloy containing 304 l stainless steel at 1000°C was chosen as the working material in the rest of this research in order to obtain more realistic and more useful results for factory practice. The effective-stress–effective-strain curve of this stainless steel is shown in Fig. 7 [12]. At high temperature, the steel is sticky so that the coefficient of friction in the interface between the rollers and the steel was taken as $\mu = 0.5$ [13].

2.4. Contact analysis between the roller and the workpiece

From the above considerations, an input file for the finite element analysis was constructed. After several trials, it was found that the initial contact condition is a crucial factor that influences the ability of the roller to grip the workpiece. Therefore, it was necessary to obtain more information about the initial contact condition between the rollers and the workpiece.

The initial contact condition between the rollers and the workpiece may be either point contact or line contact depending upon the combinations of the inclined angle and the offset angle. At the beginning of simulations, a boundary condition was used to push the workpiece forward to contact the roller. The contact area increased as the advance distance of workpiece increased. This boundary condition was removed after sufficient friction force had been built up with increased contact area. The rollers could then bite and drive the steel rod into the rolling process. If the leading end of the steel rod was preformed to a certain shape, this initial contact condition could be established very easily.

By observing the geometrical relationship of the roller and the workpiece, it was found that because the initial surface of the workpiece can be formed by a curve rotating around the X_0 axis, the normal vector of any point on the workpiece surface will pass through the center axis. A similar condition occurs to the rollers also. Thus on the initial contact point, the normal vector must simultaneously pass through the axis of the workpiece and the axis of the roller.

$\boldsymbol{R}_R$ can be represented as $\boldsymbol{R}_0$ in the coordinate system S_0 (Eqs. (6) and (7)), therefore the normal vector $\boldsymbol{N}$ of $\boldsymbol{R}_0$ can be represented as

$$\boldsymbol{N} = \boldsymbol{N}(N_x, N_y, N_z) = \frac{\partial \boldsymbol{R}_0}{\partial u} \times \frac{\partial \boldsymbol{R}_0}{\partial \theta} \tag{8}$$

It is assumed that $\boldsymbol{R}_0$ is the contact point between the roller and the workpiece and that the corresponding normal vector extends through a point $\boldsymbol{M}$ on the axis of the workpiece. The coordinate of $\boldsymbol{M}$ is

$$\boldsymbol{M} = [\, x_m \quad 0 \quad 0 \quad 1 \,]^{\mathrm{T}} \tag{9}$$

where x_m is a constant.

Thus the vector from $\boldsymbol{M}$ to $\boldsymbol{R}_0$ can be written as

$$\frac{x_m - x}{N_x} = \frac{0 - y}{N_y} = \frac{0 - z}{N_z} \tag{10}$$

Then,

$$f(u, \theta) = N_z y - N_y z = 0 \tag{11}$$

The equation above is called the Equation of Meshing [14]. From Eq. (11), we have

$$z = y \frac{N_y}{N_z} \tag{12}$$

If there exists $x_m = x(u)$, the corresponding θ, y and z can be obtained. Then the distance from the contact point to the axis of the workpiece is

$$\rho_m = \sqrt{y^2 + z^2} = |y| \sqrt{1 + \left(\frac{N_y}{N_z}\right)^2} \tag{13}$$

By linking each contact point, a contact line can be obtained. Rotating this contact line around the axis of workpiece, one can generate a perform profile for the workpiece, which can perfectly fit to the roller through contact. A similar procedure can be used to derive a special profile of the roller if the deformation of the workpiece is pre-given.

3. Discussion of simulation results

3.1. Comparison with experiment results

PSW rolling with plasticine was first simulated and the results were compared with the experimental data [7] to testify the correctness of the numerical procedures. The offset angle and inclined angle were 4° and 55°, respectively. The diameters of workpieces were reduced to 37 mm from five different initial sizes, i.e. 60, 65, 70, 75 and 80 mm. The rolling load related to the reduction in diameters is shown in Fig. 8. The loads from simulation are a little higher than those of the experiments but the trend is very close. The difference between simulation and experiment should be mainly in the properties of plasticine. In addition, the effect of the offset angles on the exiting velocity of the rod is shown in Fig. 9. The inclined angle here was set to 55° and the diameters of rods were deformed from 75 to 35 and 45 mm. The simulation results are close to those of the experiments and indicate that the exiting velocity increases with increasing offset angle.

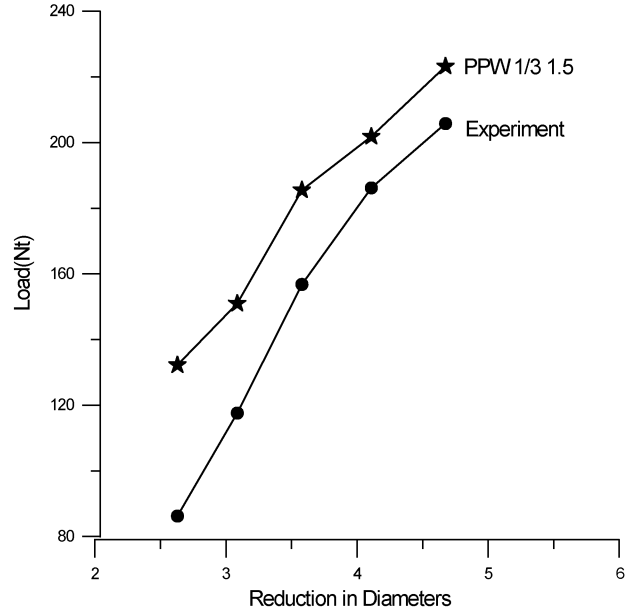

Fig. 8. Comparisons of rolling loads.

3.2. Contact analysis

The profile of a typical PSW roller can be described by two straight lines as shown in Fig. 10(a). Fig. 10(b) shows the generated profile of a workpiece corresponding to this roller. The inclination and offset of the roller lead to

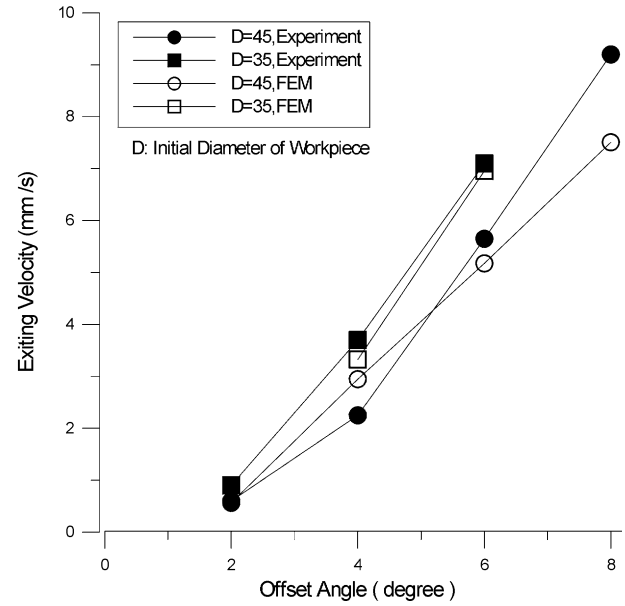

Fig. 9. Comparisons of exiting velocity.

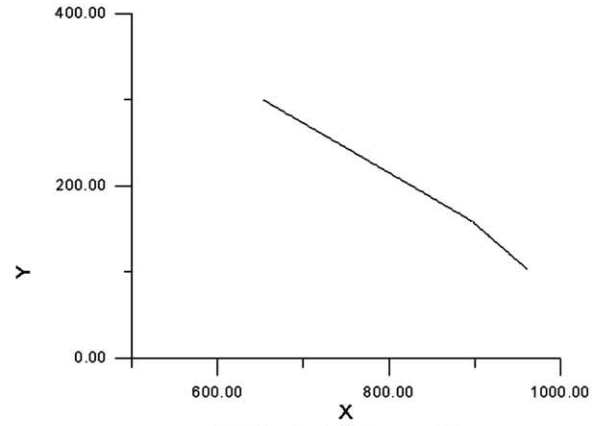

(a) Typical roller profile

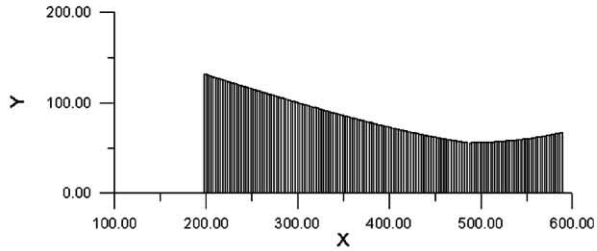

(b) Generated workpiece profile

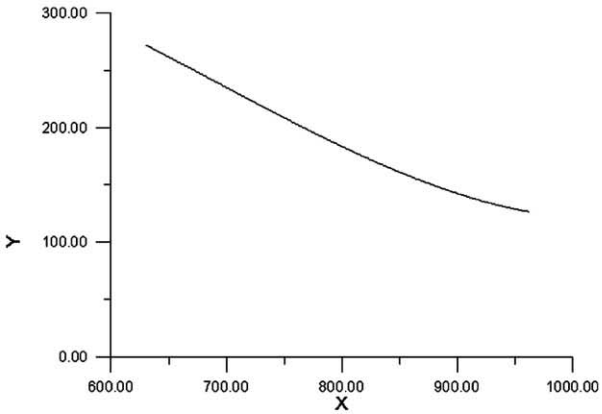

(c) Roller profile described by
$= 1.57874 \times 10^{-6} x^3 - 0.00326815x^2 + 1.71973x + 90.9101$

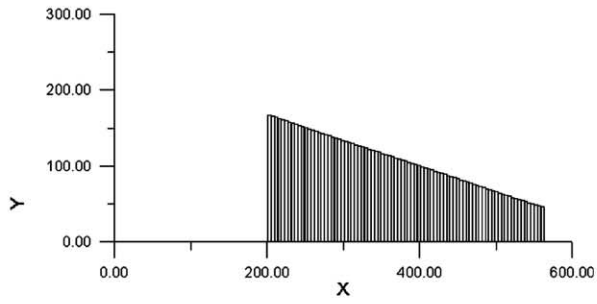

(d) Generated workpiece profile

Fig. 10. Roller profile and generated front end profile of the workpiece (mm): (a) a typical roller profile; (b) the generated workpiece profile; (c) the roller profile described by $y = 1.57874 \times 10^{-6}x^3 - 0.00326815x^2 + 1.71973x + 90.9101$; (d) the generated workpiece profile.

a V-shape profile for the workpiece. In reality, the right-side part of the V-shape will never occur, instead, a horizontal straight line will replace it because this represents the part of the workpiece that has gone through deformation. If the cross-section of the roller is described as in Fig. 10(c), the generated profile of the roller will be a straight line as in Fig. 10(d).

By observing Fig. 10(a) and (b), it can be found that the front part of the roller usually will not contact the deformed workpiece during rolling. The remaining part of the roller that deforms the workpiece through contact is called the deforming zone [7]. If the roller can be carefully arranged in such a way that makes the deformed workpiece remain constrained by the front part of the roller, the deformed shape will be retained and the workpiece will move forward smoothly before departing from the roller. This special front part of roller is then called the smoothing zone.

Based on these characteristics and using the Equation of Meshing, the front part profile of the roller can be modified to make the smoothing zone perfectly fit to the deformed workpiece to assure the accurate radius of the workpiece through the rolling process.

3.3. Deformation of the workpiece

The vertical cross-section of a deformed workpiece is shown in Fig. 11. The workpiece was twisted by the rotation of the rollers. In addition, it can be observed that the flow velocity was not uniform between the internal and external part of the material. The faster flow velocity of the external part results in a cavity condition in the leading end of the milled steel rods. Fig. 12 shows the locus of a point on the workpiece during deformation simulation. Because of the rotation of the roller and the effect of the offset angle, a point on the workpiece rotates around the axis and moved forwards simultaneously. Comparing this spiral-like profile of the locus with the generated profile for the workpiece, as shown in Fig. 10, the use of the Equation of Meshing can be validated in the contact analysis.

3.4. Rotational speed of roller

The exit velocity of the workpiece is affected by the rotational speed of the roller in conventional rolling and in the planetary rolling process also. A roller with an inclined angle $\beta = 50^\circ$ and an offset angle $\alpha = 8^\circ$ was chosen. This combination of roller parameters would reduce the radius of the rolled rod from 100 to 40 mm. The relation between the rotational speed of the roller and the exit velocity of the

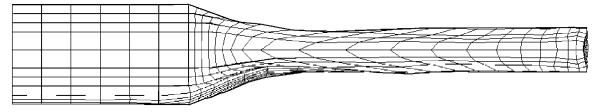

Fig. 11. Cross-section of a deformed workpiece.

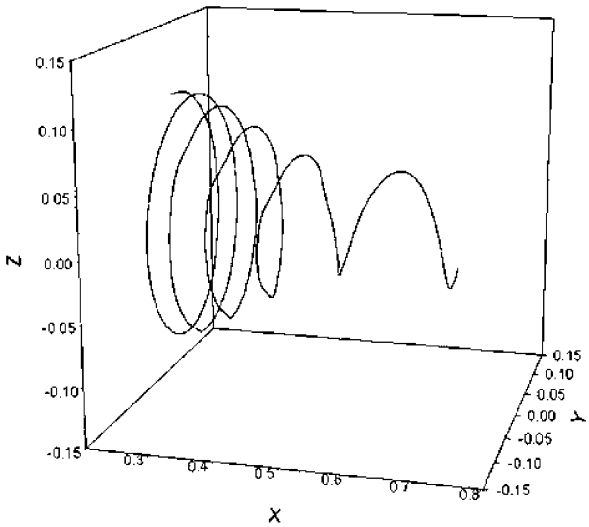

Fig. 12. Locus of a point on the workpiece (m).

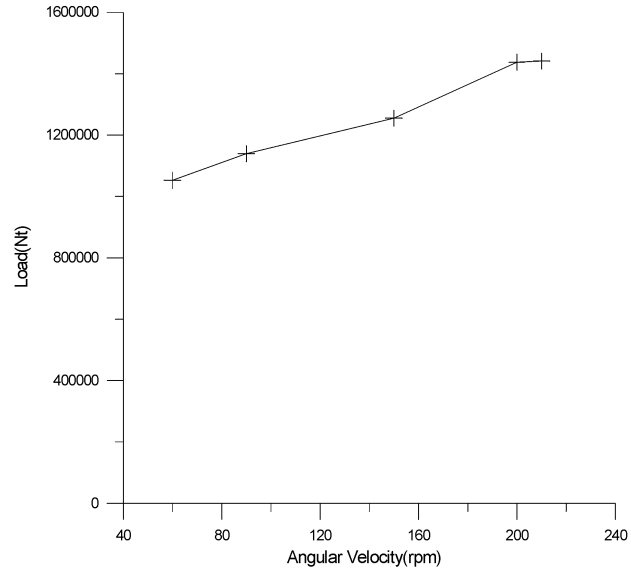

Fig. 14. Relation between the rotational speed of the roller and the rolling load.

workpiece in PSW was observed and is plotted in Fig. 13. It was found that the exit velocity of the workpiece increases as the rotational speed of the roller increases. Fig. 14 further shows that the rolling load is raised when the rotational speed is increased.

3.5. Offset angle

In the PSW, the offset angle of the roller has an important effect on the exit velocity of the deformed workpiece. For this analysis, the radius of the workpiece was reduced from 100 to 40 mm with 150 rpm as the rotational speed of the roller. The inclined angles were set to 50° and 55°, which are typical values for industrial practice.

Fig. 15 shows the exit velocity of the workpiece related to different offset angles. It is clear that the exit velocity increased as the offset angle increased for both inclined angles. With the same offset angle, the roller with a 50° inclined angle resulted in a faster exit velocity for the workpiece than that for a 55° inclined angle.

From the geometric point of view, the increase of the offset angle with the same inclined angle increases the velocity component in the forward direction of the workpiece. Contrarily, the increase of inclined angle with the same offset angle will decrease the forward velocity component and hence the exit velocity of the workpiece. The

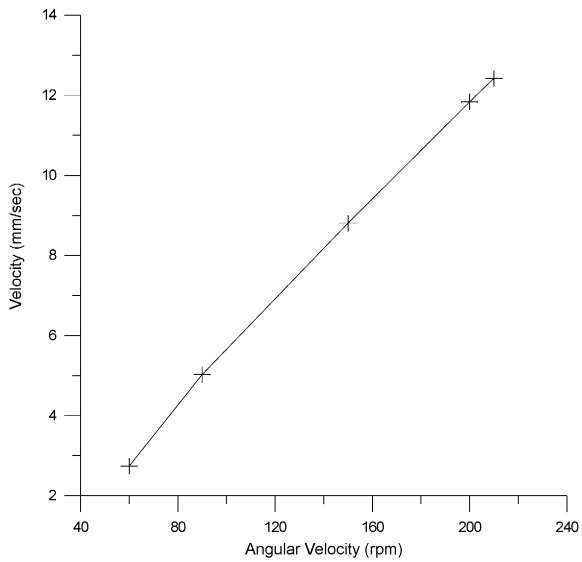

Fig. 13. Relation between the rotational speed of the roller and the exit velocity of the workpiece.

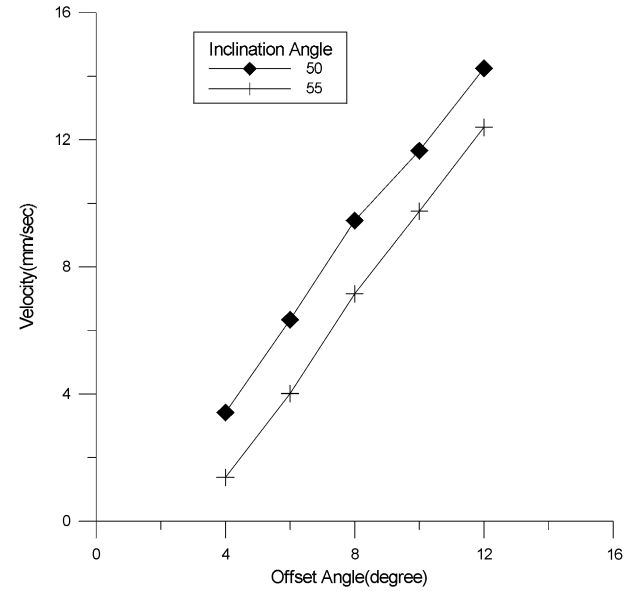

Fig. 15. Relation between the offset angle and the exit velocity of the workpiece.

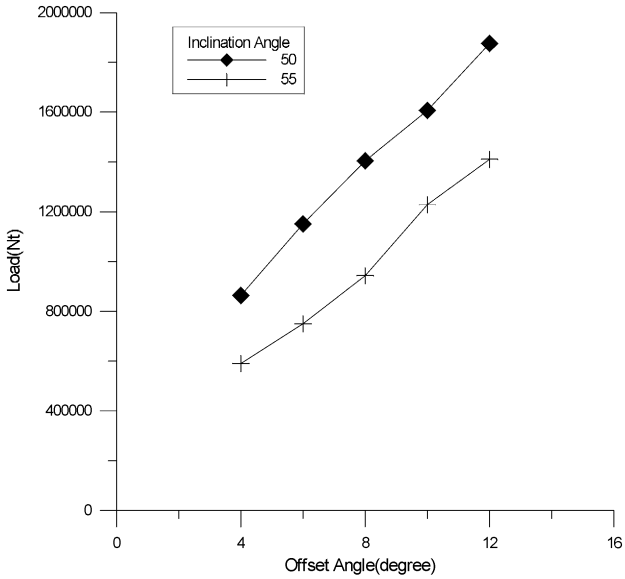

Fig. 16. Relation between the offset angle and the rolling load.

same results can be found in Aoyagi's experiments [7]. In addition to the discussed feature that the rolling load increased with the exit velocity, it also increased with the offset angle but decreased with the inclined angle as shown in Fig. 16.

3.6. Stress and strain

Figs. 17 and 18 are the contours of effective stress and effective strain of the workpiece during the rolling process. It can be seen that the maximum von Mises stress occurs at the part that is beginning to make contact with the roller. The magnitude of this stress will decrease a little at the later stages of rolling.

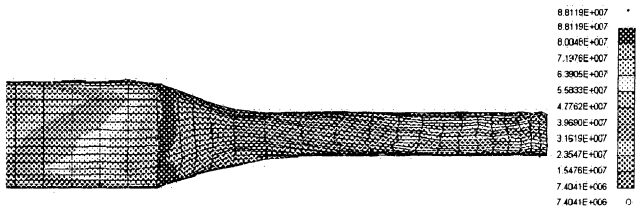

Fig. 17. von Mises stress distribution in the workpiece (Pa).

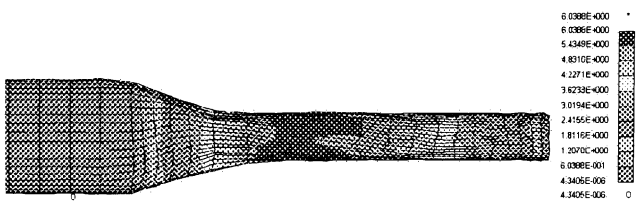

Fig. 18. Effective strain distribution in the workpiece.

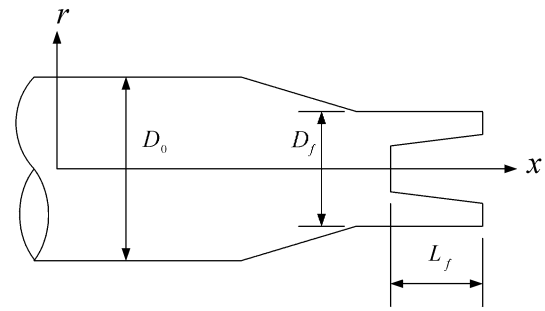

Fig. 19. Cavity in the leading end of the workpiece.

4. Optimum design

The authors have discussed the inhomogeneous deformation in the workpiece and the resulting cavity in the leading end of the workpiece (Fig. 19). If the magnitude (depth) of the cavity is significant, additional time and cost will be needed to remove it after rolling. Hence, how to choose appropriate parameters that can minimize the depth of the cavity becomes an important task. In order to handle the combined influence of several parameters to the formation of cavity, the optimum design computer code MOST [15] was integrated with the finite element code DYNA3D and the following analysis was conducted.

4.1. Object function and design variables

During the rolling process, the deformation behavior is affected not only by the material properties but also by the inclined angle and offset angle of the rollers. We have discussed the influences of both angles on rolling load and exit velocity in the above sections. In this section, we will use the optimization techniques to analyze the influence of the inclined angle and offset angle upon the cavity in the leading end of the rolled rods. Since our goal is to minimize the depth of the cavity, the object function can be written as

$$f = \min(\Delta L_f) \tag{14}$$

The value of ΔL_f is calculated from the difference between the central point and the average of ten most salient points around the end edge (see Fig. 19).

The design variables of this object function were the inclined angle β and the offset angle α. The typical values chosen for β were 50° and 55°, and occasionally 60°. Thus, the range of the inclined angle was limited to from 50° to 60°. In order to provide enough forward velocity component, the offset angle was arranged to be between 4° and 15°. The constraints of design variables were written as

$$50^\circ \le \beta \le 60^\circ, \qquad 4^\circ \le \alpha \le 15^\circ \tag{15}$$

During analysis, the shape of the deforming zone was unchanged. The shape of the smoothing zone was changed corresponding to the variance of the design variables. However, the total length of the roller axis was fixed. The radius

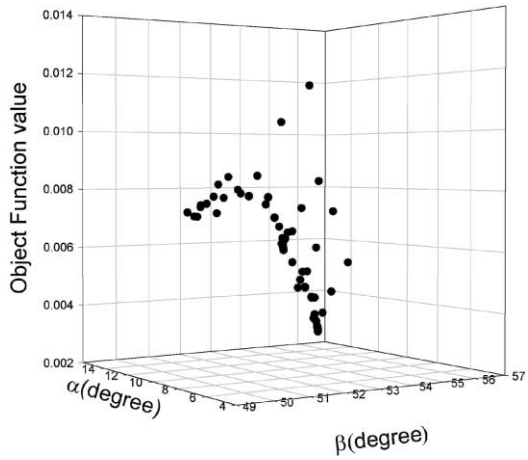

Fig. 20. Distribution of the object function values.

of the workpiece was reduced from 100 to 40 mm. The exit lengths at each analysis were not controllable because different offset angles resulted in different exit velocity of the workpiece. However, it was found that after the rolling processes had approached steady state, the cavity did not change any further. Thus the rolling time interval was restricted to that within which the deformation had become stable. In addition, the rotational speed of the roller was also fixed.

4.2. Results of optimization

An optimum solution of $\Delta L_f = 3.771$ mm was obtained with an inclined angle of $\beta = 52.25^\circ$ and an offset angle of $\alpha = 6.25^\circ$ under the above constrained conditions. Fig. 20 shows the distribution of the object function values corresponding to different combinations of design variables. The cavity was enlarged as the inclined angle and offset angle were both increased. When the offset angle was decreased, the object decreased correspondingly, but if the offset angle was too small, the workpiece would not reach a stable condition. As discussed in the previous section, the offset angle affects the exit velocity of the workpiece, so a small offset angle will give a small forward rolling speed, and the rolling process will not reach the steady state condition within the given time interval.

5. Conclusions

This research tried to provide the solution to the problem on the planetary rolling process by using the finite element method and optimum design scheme. The following conclusions were drawn:

1. The geometric model of PSW has been built by using the coordinate transformation method. In addition, the finite element simulation model has been reasonably simplified to help in reducing the complexity of the model and the computational cost.
2. The Equation of Meshing was adopted to generate the preform profile of the workpiece that contacts perfectly with the roller and vice versa. It also helped to create maximum contact area between the workpiece and the roller at the initial rolling stage. In addition, the moving locus of a point on the workpiece verified the validity of using the Equation of Meshing in generating suitable profiles for the roller or the workpiece.
3. The non-uniform flow of the workpiece led to inhomogeneous deformation, which resulted in a twisted workpiece and the formation of an end cavity. The cavity in the leading end of the rod can be successfully minimized by selecting optimum process parameters.
4. The rotational speed, offset angle and inclined angle of the roller influence the exit velocity of the workpiece and the rolling load. Increasing the rotational velocity and offset angle while decreasing the inclined angle could increase the efficiency of the rolling process, but would increase the rolling load at the same time.

From the above conclusions, certain advances in the numerical analysis of the planetary rolling process have been obtained. However, there are still topics need to be studied:

1. Simulations of the planetary rolling process on high-alloy containing stainless steels, such as 308 and 309, are worth studying because these materials have been causing problems in the industrial practice. During the rolling process with PSW, a concentrated shear zone usually results in fracture of high-alloy containing stainless steel rods. Detailed stress information obtained from finite element analysis might help in solving this problem.
2. Besides the analyzed design variables, other variables should be taken into account simultaneously. For example, the rotational speed of the roller and the material properties of the roller and workpiece will be added to further analysis by the authors in the near future.

Acknowledgements

The authors would like to thank the National Science Council of the Republic of China for its support of this work through Grant No. NSC-88-2212-E-009-003. The authors would also like to thank Prof. C.H. Tseng for offering the optimization code.

References

[1] H. Marten, New approaches in plant technology to increase quality and productivity, MPT Metall. Plant Technol. 9 (5) (1986) 39–55.
[2] W.J. Ammerling, H. Brauer, Application of 3-roll technology for rolling specialty rod and bar products, Iron Steel Eng. 65 (9) (1988) 22–27.

[3] W.J. Ammerling, Kocks 3-roll technology for high precision specialty rod and bar product, MPT Metall. Plant Technol. 12 (6) (1989) 14–19.
[4] C. Recalcati, C. Ventura, W. Rensch, HRM high-reduction rolling machine, Wire Ind. 57 (673) (1990) 31–34.
[5] Y.M. Hwang, C.W. Chang, S.J. Wu, H.B. Chen, Analysis of planetary 3-roll rolling process, Report 1, Evaluation of rolling force torque, in: Proceedings of the 19th National Conference of Theoretical and Applied Mechanics, Taiwan, ROC, 1995, pp. 165–170.
[6] Y.M. Hwang, H.H. Hsu, G.Y. Tzou, A study of PSW rolling process using stream functions, J. Mater. Process. Technol. 80–81 (1998) 341–344.
[7] K. Aoyagi, K. Ohta, Material deformation, rolling load and torque in 3-roll planetary mill, J. JSTP 24 (273) (1983) 1039–1047.
[8] T. Nishio, T. Noma, S. Karashige, H. Hino, T. Tsuta, K. Kadota, Development of three-roll planetary mill (PSW), Kawasaki Steel Tech. Rep. 84 (1995) 81–90.
[9] Y.J. Li, Elastoplastic analysis of high reduction machine of 3-roll planetary mill by the finite element method, Master Thesis, National Sun Yat-sen University, ROC, 1995.
[10] J.O. Hallquist, LS-DYNA3D Theoretical Manual, Livermore Software Technology Corporation, 1991.
[11] E. Erman, N.M. Medei, A.R. Roesch, D.C. Shan, Physical Modeling of Blocking Process in Open-die Press Forging, Bethlehem Steel Corporation, 1987.
[12] H.E. Boyer, Atlas of Stress–Strain Curves, ASM International, Metals Park, OH, 1987.
[13] E.M. Mielnik, Metalworking Science and Engineering, McGraw-Hill, New York, 1993.
[14] F.L. Litvin, Gear Geometry and Applied Theory, Prentice-Hall, Englewood Cliffs, NJ, 1994.
[15] C.H. Tseng, MOST 1.1 Manual, Technical Report No. AODL-9-96-01, Department of Mechanical Engineering, National Chiao Tung University, Taiwan, ROC, 1996.